

North-South Neutrino Heating Asymmetry in Strongly Magnetized and Rotating Stellar Cores

Kei Kotake¹, Shoichi Yamada², and Katsuhiko Sato^{1,3}

¹*Department of Physics, School of Science, University of Tokyo, 7-3-1 Hongo, Bunkyo, Tokyo 113-0033, Japan*

kkotake@utap.phys.s.u-tokyo.ac.jp

²*Science & Engineering, Waseda University, 3-4-1 Okubo, Shinjyuku, Tokyo, 169-8555, Japan*

³*Research Center for the Early Universe, University of Tokyo, 7-3-1 Hongo, Bunkyo, Tokyo 113-0033, Japan*

ABSTRACT

We perform a series of two-dimensional magnetohydrodynamic simulations of supernova cores. Since the distributions of the angular momentum and the magnetic fields of strongly magnetized stars are quite uncertain, we systematically change the combinations of the strength of the angular momentum, the rotation law, the degree of differential rotation, and the profiles of the magnetic fields to construct the initial conditions. By so doing, we estimate how the rotation-induced anisotropic neutrino heating are affected by the strong magnetic fields through parity-violating effects and first investigate how the north-south asymmetry of the neutrino heating in a strongly magnetized supernova core could be. As for the microphysics, we employ a realistic equation of state based on the relativistic mean field theory and take into account electron captures and the neutrino transport via the neutrino leakage scheme. With these computations, we find that the parity-violating corrections reduce $\lesssim 0.5\%$ of the neutrino heating rate than that without the magnetic fields in the vicinity of the north pole of a star, on the other hand, enhance about $\lesssim 0.5\%$ in the vicinity of the south pole. If the global asymmetry of the neutrino heating in the both of the poles develops in the later phases, the newly born neutron star might be kicked toward the north pole in the subsequent time.

Subject headings: supernovae: collapse, rotation—magnetars: pulsars, magnetic field

1. Introduction

Neutron stars are created in the aftermath of the gravitational core collapse of massive stars at the end of their lives. After the supernova explosions, the nascent neutron stars receive the rapid rotations and large magnetic fields, which are believed to be observed as pulsars. Thus, rotations and magnetic fields should be naturally taken into account in order not only to clarify the explosion mechanism, but also to explain the observed properties of neutron stars. Here it is noted that the number of studies including such multidimensional aspects is increasing recently (Akiyama et al. 2003; Buras et al. 2003; Kotake, Yamada, & Sato 2003; Kotake et al. 2004; Ott et al. 2003; Kotake, Yamada, & Sato 2003; Yamada & Sawai 2003; Kotake et al. 2004; Fryer & Warren 2004; Müller et al. 2004; Yamada, Kotake, & Yamasaki 2004; Liebendörfer et al. 2004). This may reflect the fact that only the neutrino heating mechanism assuming spherical symmetry seems difficult to produce the explosions (Rampp & Janka 2000; Liebendörfer et al. 2001; Thompson, Burrows, & Pinto 2003; Liebendörfer et al. 2003).

Among the unresolved mysteries in context of core-collapse supernovae, the physical origin of the pulsar kicks has been long controversial. Recent analyses of individual pulsar motions and observations of remnant associations between supernovae and pulsars indicate that supernovae explosions are asymmetric and that the neutron stars receive large kick velocities at birth (typically 300 – 400 km/s (Lyne & Lorimer 1994; Lorimer, Bailes, & Harrison 1997), with highest values greater than 1000 km/s (Arzoumanian, Chernoff, & Cordes 2002)). The existence of pulsar kicks are also supported by the evolutionary studies of neutron star and black hole binaries (Fryer & Kalogera 1997; Wex, Kalogera, & Kramer 2000; Mirabel et al. 2002) and by the detections of geodetic and orbital plane precessions in some binary pulsars (Cordes, Wasserman, & Blaskiewicz 1990; Kapsi et al. 1996). The recent X-ray observations have shown the correlation between the direction of pulsar motions and the spin axis of their supernovae in Vela and Crab pulsars (Helfand, Gotthelf, & Halpern 2001; Pavlov et al. 2001). However it is statistically uncertain whether the spin-kick alignment is a generic feature of all pulsars.

So far two major classes of mechanism for these kicks have been suggested (see Lai, Chernoff, & Cordes (2001); Lai (2004) for a review). Any models or mechanisms should explain how the explosions become asymmetric and how the generated asymmetric explosions are related to the formation of the pulsar kicks. The first class of the mechanisms relies on the asymmetric explosion as a result of the global convective instabilities (Burrows & Hayes 1996; Goldreich et al. 1996) caused by the pre-collapse density inhomogeneities (Bazan & Arnett 1998) or the local convective instabilities (Janka & Mueller 1994) formed after the onset of core-collapse. More recently, Scheck et al. (2004) reported in their two dimensional

simulations that in the long duration explosions (more than a second after bounce), the neutrino-driven convections behind the expanding shock can lead the global asymmetries, which accelerates the remnant neutron star to a several hundreds of km/s (see, also Fryer (2004) for three dimensional calculations). In their simulations, the central protoneutron star is fixed as the inner boundary condition. Fully self-consistent calculations are required to confirm whether this assumption is valid or not.

Here we pay attention to the second class of models in which the pulsar kicks arise from an asymmetry of neutrinos induced by the strong magnetic field ($B \geq 10^{15}$ G) in the collapsed supernova core. While the dipolar magnetic fields of most radio pulsars are observed to lie in the range of $10^{12} \sim 10^{13}$ G, several recent observations imply that the soft gamma-ray repeaters and anomalous X-ray pulsars have the strong magnetic fields as high as $B \sim 10^{15}$ G (Zhang & Harding 2000; Guseinov et al. 2003). So far, much theoretical efforts have been paid to formulate the neutrino opacity in such a strong magnetic fields (Horowitz & Li (1998); Arras & Lai (1999), Arras & Lai (1999)). On the other hand, it seems that little attention has been paid to investigate how the asymmetric neutrino heatings work globally in the supernova core based on the numerical simulations. In addition, most of the preceding studies relies on the asymmetry of the neutrinos only by the magnetic fields (see, however, Janka & Raffelt (1999); Duan & Qian (2004) for the simple models of atmosphere in the supernova core). It is noted that rotation should also contribute to produce the asymmetry of the neutrino heating (Kotake, Yamada, & Sato 2003). To our knowledge, the degree of the neutrino heating asymmetry under the presence of the rotation and the strong magnetic fields at the same time has not been investigated so far. This situation leads us to investigate how the rotation-induced anisotropic neutrino heating (Kotake, Yamada, & Sato 2003) are affected by the strong magnetic fields through parity-violating effects. In this study, we perform a series of two-dimensional simulations of magnetorotational core collapse. In order to see the parity-violating effects, we pay particular attention to the models, which are assumed to have the strong poloidal magnetic fields ($\sim 10^{12}$ G) prior to core-collapse. Since the profiles of the angular momentum and the magnetic fields of such strongly magnetized stars are still quite uncertain (see, however, Heger et al. (2003)), we change the strength of the rotation and the magnetic fields systematically. Based on the simulations from the onset of the core-collapse through the bounce to the shock-stall, we demonstrate how large the anisotropy of neutrino heating could be globally in the supernova core. Furthermore, we hope to speculate their possible effects on the pulsar kicks.

We describe the numerical methods in section 2. The main numerical results are shown in section 3. Discussion are given in section 4. We conclude this paper in section 5.

2. Numerical Methods and Initial Models

The numerical method for magnetohydrodynamic (MHD) computations employed in this paper is based on the ZEUS-2D code (Stone & Norman 1992). The ZEUS-2D is an Eulerian code based on the finite-difference method and employs an artificial viscosity of von Neumann and Richtmyer to capture shocks. The time evolution of magnetic field is solved by the induction equation : $\partial \mathbf{B} / \partial t = \nabla \times (\mathbf{v} \times \mathbf{B})$, with \mathbf{v} , \mathbf{B} being velocity and the magnetic field, respectively. In so doing, the code utilizes the so-called constrained transport (CT) method, which ensures that the numerically evolved magnetic fields are divergence-free ($\nabla \cdot \mathbf{B} = 0$) at all times. Furthermore, the method of characteristics (MOC) is implemented to propagate accurately all modes of MHD waves. The self-gravity is managed by solving the Poisson equation with the incomplete Cholesky decomposition conjugate gradient method. In all the computations, spherical coordinates are used and one quadrant of the meridian section is covered with 300 (r) \times 50 (θ) mesh points. We have made several major changes to the base code to incorporate the microphysics. First, we added an equation for the electron fraction to treat electron captures and neutrino transport by the so-called leakage scheme (Epstein & Pethick 1981; Bludman et al. 1982; Van Riper & Lattimer 1981; Van Riper 1982). The calculation of electron fraction is done separately from the main hydrodynamic step in an operator-splitting manner. Second, we implemented a tabulated equation of state based on the relativistic mean field theory (Shen et al. 1998) instead of the ideal gas EOS assumed in the original code. For a more detailed description of the methods, see Kotake, Yamada, & Sato (2003).

2.1. Initial Conditions

Recently, Heger et al. (2003) performed the most up-to-date stellar evolution calculations including the effects of rotation, mixing, transport of the angular momentum, and the magnetic torques. Their models show that the toroidal magnetic fields are much stronger than the poloidal ones prior to core collapse. In our previous paper (Kotake et al. 2004), we considered such models as the initial conditions. However, if such initial configurations are true, no parity-violating effects of the magnetic fields on the neutrino heating can be obtained in the two-dimensional axisymmetric simulations. Considering the uncertainties in Heger’s evolution calculations that they are one-dimensional models, which hinder the accurate treatment of the transport of the angular momentum and the generation of the magnetic fields, it should be still important to take the poloidal magnetic fields as the initial conditions. Thus in this study, we choose to assume that only the poloidal magnetic fields exist prior to core-collapse, and then, prefer a parametric approach to construct the

initial conditions varying the profiles of the initial poloidal magnetic fields. We assume the following two rotation laws and the four configurations of the magnetic fields.

1. shell-type rotation:

$$\omega(r) = \omega_0 \times \frac{R_0^2}{r^2 + R_0^2}, \quad (1)$$

and shell-type magnetic fields,

$$B(r) = B_0 \times \frac{R_0^2}{r^2 + R_0^2}, \quad (2)$$

where $\omega(r)$ is an angular velocity, $B(r)$ is the poloidal component of the magnetic fields, r is radius, and ω_0, R_0 and B_0 are model constants,

2. cylindrical rotation:

$$\omega(X, Z) = \omega_0 \times \frac{X_0^2}{X^2 + X_0^2} \cdot \frac{Z_0^4}{Z^4 + Z_0^4}, \quad (3)$$

and cylindrical magnetic fields,

$$B_z(X, Z) = B_0 \times \frac{X_0^2}{X^2 + X_0^2} \cdot \frac{Z_0^4}{Z^4 + Z_0^4}, \quad (4)$$

and uniform cylindrical magnetic fields,

$$B_z = B_0, \quad (5)$$

where B_z is the poloidal magnetic fields parallel to the rotational (Z) axis, X and Z denote distances from the rotational axis and the equatorial plane and X_0, Z_0 are model constants. The other parameters have the same meanings as above.

Finally, we take into account the quadrupole magnetic fields following the prescription by Ardeljan, Bisnovaty-Kogan, & Moiseenko (1998),

$$\begin{aligned} B_x(X, Z) &= F_x(0.5\hat{X}, 0.5\hat{Z} - 2.5) - F_x(0.5\hat{X}, 0.5\hat{Z} + 2.5), \\ B_z(X, Z) &= F_z(0.5\hat{X}, 0.5\hat{Z} - 2.5) - F_z(0.5\hat{X}, 0.5\hat{Z} + 2.5), \end{aligned} \quad (6)$$

with

$$\hat{X} = \frac{X}{X_{0,\text{quad}}}, \quad \hat{Z} = \frac{Z}{Z_{0,\text{quad}}}, \quad (7)$$

and

$$\begin{aligned} F_x(\hat{X}, \hat{Z}) &= B_0 \left(\frac{2\hat{X}\hat{Z}}{(\hat{Z}^2 + 1)^3} - \frac{2\hat{X}^3\hat{Z}}{(\hat{Z}^2 + 1)^5} \right) \\ F_z(\hat{X}, \hat{Z}) &= B_0 \left(\frac{1}{(\hat{Z}^2 + 1)^2} - \frac{\hat{X}^2}{(\hat{Z}^2 + 1)^4} \right), \end{aligned} \quad (8)$$

where B_x is the poloidal magnetic fields parallel to the equatorial plane and $X_{0,\text{quad}}, Z_{0,\text{quad}}$ are model constants.

We have computed 11 models changing the combination of the strength of the angular momentum, the rotation law, the degree of differential rotation, and the profiles of the magnetic fields. For all the models, we fix the values of $E_m/|W|$ to be 0.1%, where $E_m/|W|$ represents the ratio of the magnetic to the gravitational energy. The model parameters are presented in Table 1. The models are named after this combination, with the first letter, “S (shell)”, “C (cylindrical)”, denoting the rotation profiles, the second letter, “L (long), S (short)”, indicating the values of R_0 and X_0 , the third letter “(U) uniform, (NU) non uniform, (Q) quadrupole” indicating the configurations of the initial poloidal magnetic field, the fourth number -1 or -2, representing that the initial $T/|W|$ is $10^{-1}, 10^{-2}\%$, respectively. Note that the ratio of rotational energy to gravitational energy is designated as $T/|W|$.

We note that our choice of the initial value of $T/|W|$ is much smaller than the past magnetorotational studies in context of core-collapse supernovae (LeBlanc & Wilson 1970; Bisnovatyi-Kogan et al. 1976; Müller & Hillebrandt 1979; Symbalisty 1984; Ardeljan et al. 2000) to reconcile with the recent stellar evolution calculations of rotating stars (Heger et al. 2000). However it is still larger than the most slowest rotating models predicted by the most recent stellar calculations (Heger et al. 2003). As for the configurations of the initial magnetic fields, we prepared a variety of them in order to cover as wide the parametric space of the field configurations as possible. As for the initial strength of the magnetic fields, we pay particular attention to the models, which are assumed to have the strong poloidal magnetic fields ($\sim 10^{12}$ G) prior to core-collapse in order to see the parity-violating effects. Astrophysically, such models are likely to associate with the formation of the so-called magnetars.

3. Results

3.1. Magnetohydrodynamic Features

We briefly summarize some dynamical aspects which will be helpful in the later discussions. For the more detailed magnetohydrodynamic computations during core-collapse, see also our accompanying paper (Takiwaki et al. 2004).

In Figure 1, the entropy distributions at the final states for some representative models are presented. The final time of all the models is about 50 ms after core bounce (see Table 1). At the final time, the shock wave produced at core bounce tends to stall in the core except for the models, which have the centrally condensed magnetic fields and rapid rotation with

Table 1. The Model Parameters.

Model	Rotation profiles	B profiles	ω_0 (s ⁻¹)	B_0 (G)	$R_0, X_0, Z_0 \times 10^8$ (cm)
SL(U)-2	Shell	Uniform Cylinder	0.6	1.9×10^{12}	$R_0 = 1$
SS(U)-2	Shell	Uniform Cylinder	9.0	1.9×10^{12}	$R_0 = 0.1$
CS(U)-2	Cylinder	Uniform Cylinder	6.3	1.9×10^{12}	$X_0 = 0.1, Z_0 = 1$
SS(NU)-2	Shell	Shell	9.0	1.1×10^{14}	$R_0 = 0.1$
CS(NU)-2	Cylinder	Cylinder	6.3	4.7×10^{13}	$X_0 = 0.1, Z_0 = 1$
SL(Q)-2	Shell	Quadrupole	9.0	1.4×10^{13}	$R_0 = 1, X_{0,\text{quad}} = Z_{0,\text{quad}} = 1.6$
CS(Q)-2	Cylinder	Quadrupole	6.3	1.4×10^{13}	$X_0 = 0.1, Z_0 = 1, X_{0,\text{quad}} = Z_{0,\text{quad}} = 1.6$
SL(U)-1	Shell	Uniform Cylinder	1.7	1.9×10^{12}	$R_0 = 1$
SS(U)-1	Shell	Uniform Cylinder	28.3	1.9×10^{12}	$R_0 = 0.1$
SL(NU)-1	Shell	Shell	1.7	5.2×10^{12}	$R_0 = 1$
SS(NU)-1	Shell	Shell	28.3	1.1×10^{14}	$R_0 = 0.1$

Note. — Note in the table that “B profiles” indicates the profiles of the initial magnetic fields. Note also that the number (-1 or -2), which each model has in its name, indicates the values of initial $T/|W|$ of $10^{-1}, 10^{-2}\%$, respectively.

Table 2. Properties of the Final States.

Model	t_f (ms)	B_p (G)	B_ϕ (G)	r_{sh}^e (km)	r_{sh}^p (km)	$T/ W _f(\%)$	$E_m/ W _f(\%)$
SL(U)-2	40.2	1.5×10^{16}	2.4×10^{15}	157	175	2.5×10^{-1}	1.9×10^{-1}
SS(U)-2	41.8	3.4×10^{16}	2.3×10^{15}	178	233	2.5×10^{-1}	1.7×10^{-1}
CS(U)-2	40.7	3.2×10^{16}	3.7×10^{15}	144	612	2.5×10^{-1}	1.7×10^{-1}
SS(NU)-2	42.5	5.2×10^{16}	1.9×10^{15}	163	148	1.1×10^{-1}	5.3×10^{-1}
CS(NU)-2	43.1	4.6×10^{16}	4.9×10^{14}	176	1471	1.1×10^{-1}	3.7×10^{-1}
SL(Q)-2	37.1	1.2×10^{16}	9.4×10^{15}	146	125	2.6×10^{-1}	5.2×10^{-2}
CS(Q)-2	46.0	3.0×10^{16}	9.3×10^{15}	169	215	3.4×10^{-1}	7.1×10^{-2}
SL(U)-1	42.3	3.0×10^{16}	6.0×10^{15}	226	573	1.4	3.8×10^{-1}
SS(U)-1	47.1	4.1×10^{16}	2.0×10^{16}	133	1361	1.8	3.6×10^{-1}
SL(NU)-1	45.0	2.7×10^{16}	4.9×10^{15}	278	444	1.0	8.3×10^{-1}
SS(NU)-1	44.4	5.8×10^{16}	7.0×10^{14}	425	1325	2.8×10^{-1}	8.6×10^{-1}

Note. — t_f represents the final time measured from core bounce. B_p and B_ϕ are the maximum strength of the poloidal and the toroidal magnetic fields, respectively. r_{sh}^e and r_{sh}^p are the distances from the center to the stalled shock front in the equatorial plane and along the rotational axis, respectively.

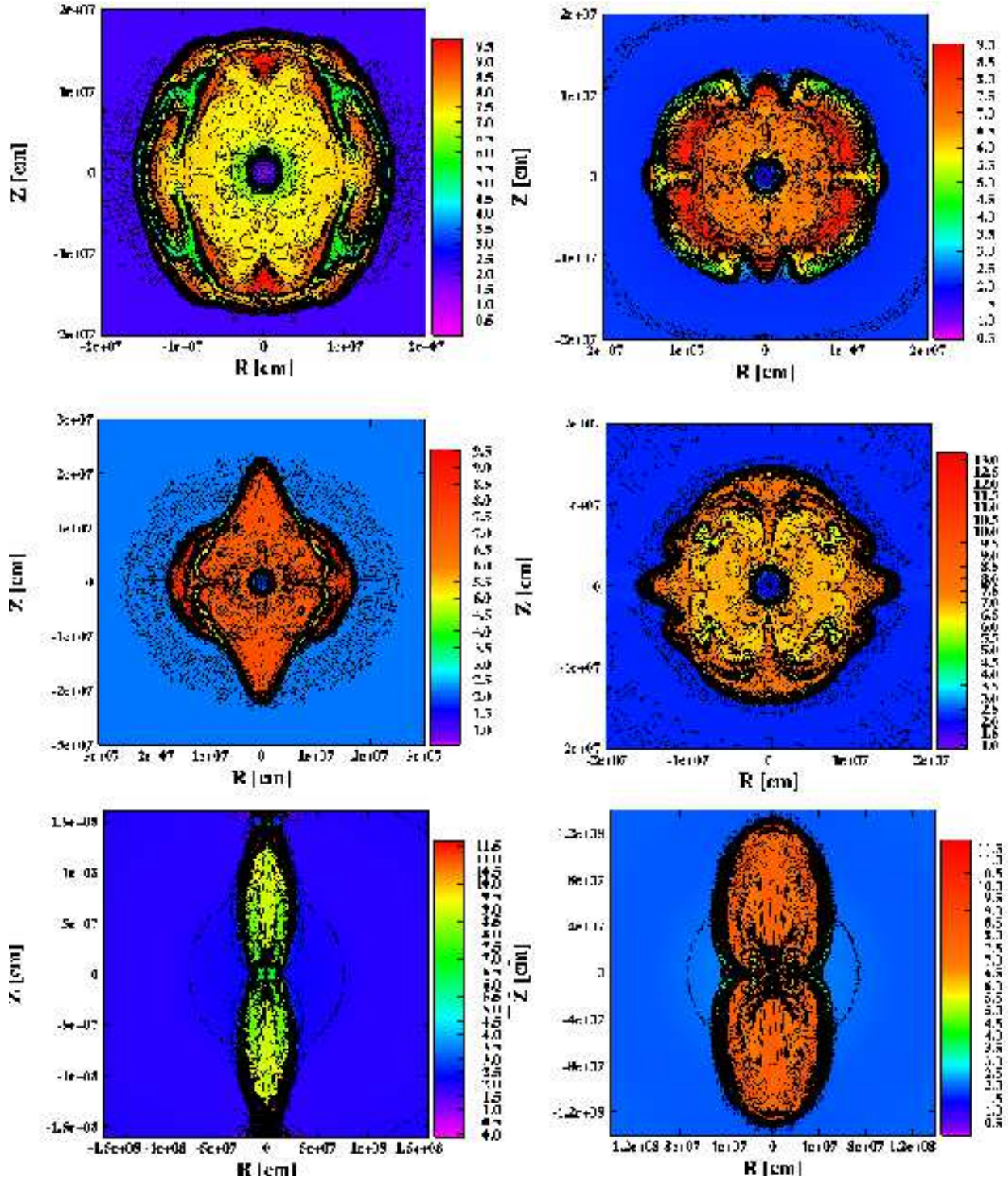


Fig. 1.— The final profiles of models SL(U)-2 (upper left), SS(Q)-2 (upper right), SS(U)-2 (middle left), SS(NU)-2 (middle right), CS(NU)-2 (lower left), SS(NU)-1 (lower right). They show color-coded contour plots of entropy (k_B) per nucleon.

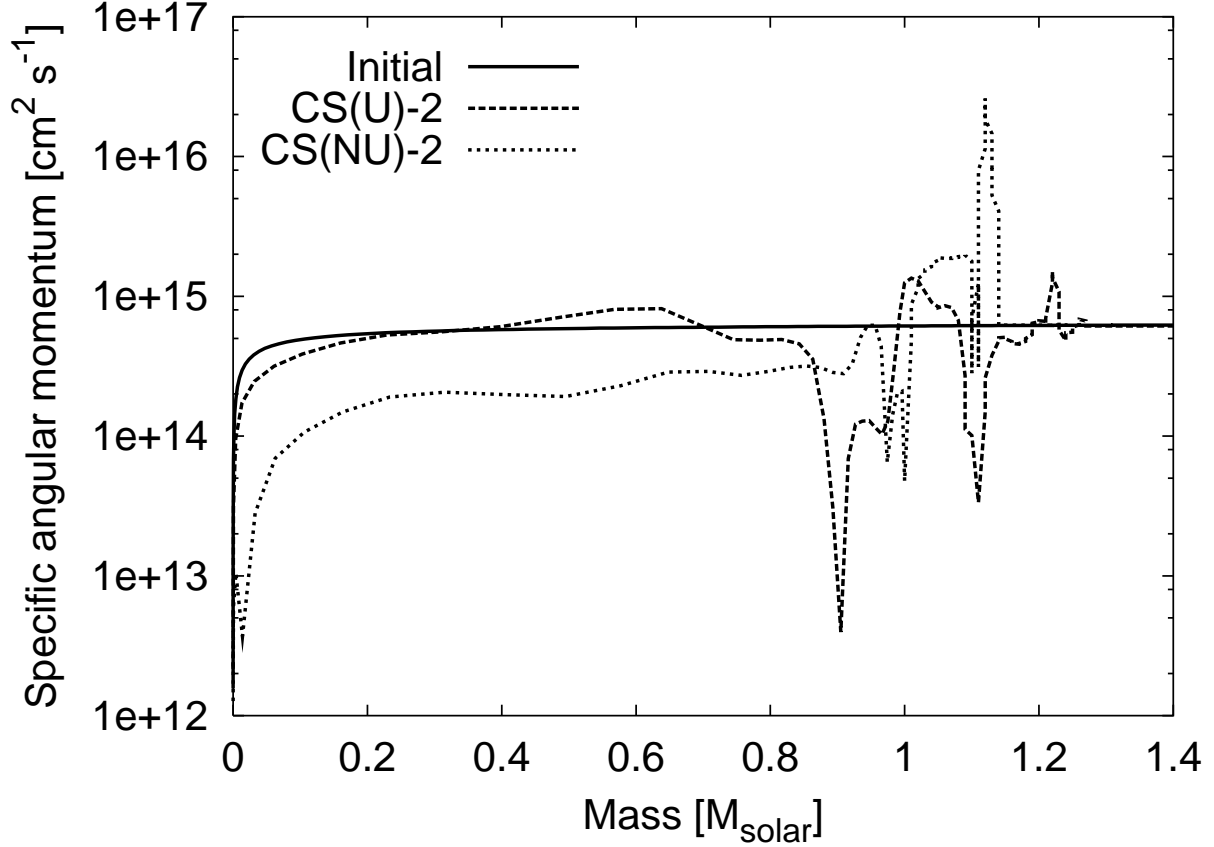


Fig. 2.— The cumulative mass vs. specific angular momentum distribution in unit of M_{\odot} for models CS(U)-2 and CS(NU)-2 at the final state. Note in the figure that 'Initial' represents the initial configuration of the specific angular momentum for the models. It is seen that the angular momentum is transferred more efficiently for the model with the centrally condensed magnetic fields profile (model CS(NU)-2) than model CS(U)-2.

Table 3. Analysis of the Heating Rate in the Strong Magnetic Fields.

Model	R_{ν^P} (km)	R_{ν^e} (km)	R_{mag} (%)
SL(U)-2	66.6	73.1	0.13
SS(U)-2	71.4	71.4	0.27
CS(U)-2	57.3	73.1	0.27
SS(NU)-2	65.1	68.2	0.08
CS(NU)-2	54.3	68.2	0.18
SL(Q)-2	69.8	68.2	0.14
CS(Q)-2	66.6	68.2	0.09
SL(U)-1	57.3	73.1	0.37
SS(U)-1	55.8	66.6	0.42
SL(NU)-1	50.0	65.1	0.26
SS(NU)-1	51.4	66.6	0.12

Note. — R_{ν^e} and R_{ν^P} are the distances from the center to the neutrino sphere, respectively. $R_{\text{mag}} = |\Delta Q_{\nu, B \neq 0}^+ / Q_{\nu, B=0}^+|$ is the maximum ratio of the neutrino heating rate contributed from the parity-violating effects, $\Delta Q_{\nu, B \neq 0}^+$ to the heating rate without the corrections, $Q_{\nu, B=0}^+$.

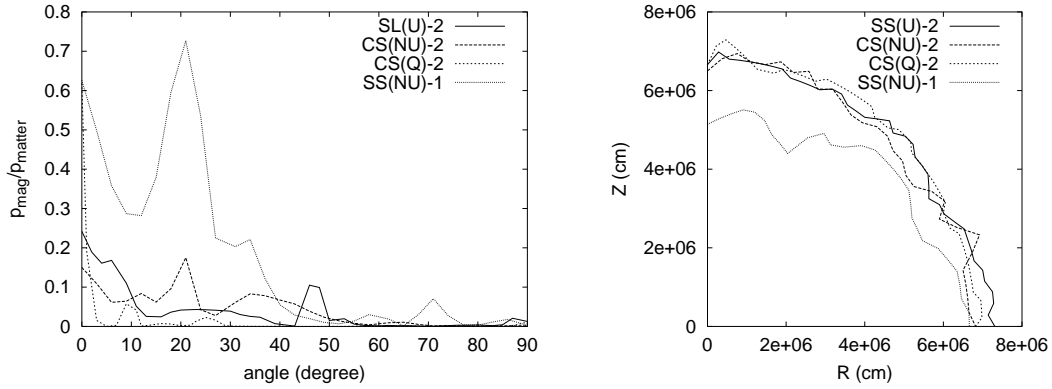


Fig. 3.— The ratio of the magnetic (p_{mag}) to the matter pressure (p_{matter}) with the polar angle on the neutrino sphere (left panel) and the shapes of the neutrino spheres for some representative models (right panel). Note in the right panel that R, Z represents the distance from the rotational axis and the equatorial plane, respectively.

the strong differential rotation initially (see Figure 1 and Table 1 for models CS(NU)-2, SS(U)-1, and SS(NU)-1). Even if the shock waves of such models manage to approach the outer boundary of the numerical simulation ($Z \sim 1500$ km) along the rotational axis, the explosion energy is about one order of magnitude less than the canonical one. Thus, the neutrino heatings in the later phases should be necessary for the successful explosions. Here it is noted that the final value of $T/|W|$'s and $E_m/|W|$'s for our models are well below the past MHD studies (Symbalisty 1984) assuming rapid rotation prior to core-collapse. Even in our slower rotating models than the previous simulations, it is found that the asymmetric matter motions can appear as seen from Figure 1.

During core-collapse, the strength of the magnetic fields exceeds the QED critical value $B_{\text{QED}} = 4.4 \times 10^{13}$ (G), above which the neutrino reactions are affected by the parity-violating corrections of weak interaction. Just before core bounce, the poloidal magnetic fields dominate over the toroidal ones due to our assumption of the initial field configuration. After core bounce, the strong differential rotations near the surface of the protoneutron star wraps the poloidal magnetic fields to convert into the toroidal ones, whose strength becomes as high as $B \sim 10^{15}$ G at the final time of the simulations. The growth of the toroidal magnetic fields can be estimated by an order-of-magnitude estimation as follows,

$$B_\phi \sim 2.0 \times 10^{15} \text{ G} \left(\frac{B_z}{10^{15} \text{ G}} \right) \left(\frac{\Delta t}{50 \text{ msec}} \right) \left(\frac{\omega}{500 \text{ rad s}^{-1}} \right), \quad (9)$$

where B_z is the typical strength of the magnetic field parallel to the rotational axis just before core bounce, Δt is the duration of the wrapping time, which is roughly equivalent to the time from core bounce to the final time, ω is the mean angular velocity at the surface of the protoneutron star. This estimation is roughly consistent with the numerical simulations. It is noted that the tangled toroidal magnetic fields ($B_\phi \lesssim 10^{16}$ G) are weaker than the poloidal ones ($B_p \gtrsim 10^{16}$ G) at the final time in our models (see Table 1). Magnetorotational instability (MRI) is another candidate to amplify the growth of the toroidal magnetic fields. Although the typical time scale (Balbus & Hawley 1998) corresponding to the maximum growth of MRI ($\tau_{\text{MRI}} \sim O(10)$ ms) at the surface of the protoneutron star is shorter than the simulation time scale (~ 50 ms), it is much longer than the growth time scale of the field wrapping ($\tau_{\text{wrap}} \sim O(1)$ ms). Thus the amplification of the toroidal magnetic fields in our models is mainly as a result of the winding up original vertical poloidal fields.

In Figure 2, the cumulative distribution of specific angular momentum is shown for models CS(U)-2 and CS(NU)-2. In the magnetorotational core-collapse, the anisotropic magnetic stress transfers the specific angular momentum of each fluid element outwards even in axisymmetry if the fluid rotates differentially. It is noted that the mass of the unshocked core is about $\sim 0.8M_\odot$ in these models. From the figure, it is found that the transport of the angular momentum occurs more efficiently for the model CS(NU)-2, whose initial magnetic

fields are more centrally condensed, than the model CS(U)-2 (compare the specific angular momentum in Figure 2). In addition, there are regions just outside the unshocked core where the specific angular momentum decreases outwards. In such regions, the so-called Rayleigh instability condition holds, which induces the convection at the later phases near the surface of the unshocked core in the equatorial plane. These differences mentioned above stem only from the degree of the initial concentration of the magnetic fields between the pair models and are common to the other pair of the models.

After the final time of our simulations, we calculate the shapes of the neutrino spheres by the prescription (Kotake, Yamada, & Sato 2003). Although the magnetic fields become strong as $B \sim 10^{15}$ G in the vicinity of the neutrino sphere ($r = 50 \sim 70$ km, density $\sim 10^{11}$ g cm $^{-3}$), the pressure of the magnetic fields ($p_{\text{mag}} \equiv \frac{B^2}{8\pi} \sim 10^{29} (B/2 \times 10^{15} \text{ G})^2 \text{ dyn cm}^{-2}$) are smaller than that of the matter ($p_{\text{matter}} \sim 10^{30} \text{ dyn cm}^{-2}$) in the corresponding region (see the left panel of Figure 3). Thus it is found that the magnetic fields do not affect the shape of the neutrino sphere significantly. In fact, the neutrino spheres are deformed to be oblate for the rapidly rotating models, on the other hand, to be rather spherical for the slowly rotating models (see the right panel of Figure 3 and compare the shape of the neutrino sphere of model SS(NU)-1 (:faster rotating model in our computation) with that of the other models (:slower rotating models)).

3.2. Effects of the strong magnetic fields on the neutrino heating

Based on the neutrino spheres obtained in the previous section, we will estimate the heating rates including the corrections from the parity-violating effects outside the neutrino sphere. This is admittedly a very crude estimate, since it is pointed out (Liebendörfer et al. 2001; Thompson, Burrows, & Pinto 2003) that the net heating, the heating minus cooling, becomes positive $\sim 50 - 100$ msec after the shock stagnation. In this respect, we confirmed that the cooling dominates over the heating also for our models including the corrections of the parity-violating effects. Since our calculations ended before the heating dominates over the cooling, it is impossible to estimate the location of the gain radius, beyond where the heating dominates over the cooling. Here it is noted that the contrast of the heating to the cooling is found to be similar in our short simulation runs. Thus, the gain radius should be also deformed in the later phase. If this feature lasts in the later phase, the bare heating rate discussed in the following and the resultant neutrino asymmetry due to the parity-violating corrections, will help to understand the net neutrino asymmetry. Hence, bearing this caveat in mind, we study the bare heating rate with the parity-violating effects for the final configurations (several tens msec after the bounce) in our simulations.

First of all, we state how we estimate the neutrino heating rate in the strongly magnetized supernova core. The analysis scheme is schematically shown in Figure 4. Neutrinos are assumed to be emitted isotropically from each point on the neutrino sphere and stream freely later on. Then the heating rate at a given point outside the neutrino sphere can be found by summing up all the rays from the neutrino sphere. The heating by electron neutrinos proceeds via the charged current interaction:

$$\nu_e + n \rightarrow p + e^- . \quad (10)$$

We employ the corresponding cross section in a strongly magnetic field given by Arras & Lai (1999), which is expressed as follows :

$$\sigma_B^{(\text{abs})} = \sigma_0^{(\text{abs})} (1 + \epsilon_{\text{abs}} \hat{\mathbf{n}} \cdot \hat{\mathbf{B}}), \quad (11)$$

where $\sigma_0^{(\text{abs})}$ is the corresponding cross section without the magnetic fields, $\hat{\mathbf{n}}$, $\hat{\mathbf{B}}$ are the unit momentum vector for the incoming neutrinos and the unit vector along the magnetic field direction (see Figure 4), and ϵ_{abs} is the asymmetry parameter given by

$$\epsilon_{\text{abs}} = \epsilon_{\text{abs}}(\text{e}) + \epsilon_{\text{abs}}(\text{np}). \quad (12)$$

Here $\epsilon_{\text{abs}}(\text{e})$ and $\epsilon_{\text{abs}}(\text{np})$ are expressed in the leading order at the neutrino energies as

$$\epsilon_{\text{abs}}(\text{e}) = \frac{1}{2} \frac{\hbar c e B}{\epsilon_\nu^2} \frac{c_V^2 - c_A^2}{c_V^2 + 3c_A^2}, \quad (13)$$

and

$$\begin{aligned} \epsilon_{\text{abs}}(\text{np}) &= 2 \frac{c_A(c_A + c_V)}{c_V^2 + 3c_A^2} \frac{\mu_{\text{Bn}} B}{k_B T} - \frac{k_B T}{\epsilon_\nu} \left[1 + \frac{\epsilon_\nu}{k_B T} \right] \\ &\times \left[2 \frac{c_A(c_A + c_V)}{c_V^2 + 3c_A^2} \frac{\mu_{\text{Bn}} B}{k_B T} + 2 \frac{c_A(c_A - c_V)}{c_V^2 + 3c_A^2} \frac{\mu_{\text{Bp}} B}{k_B T} \right], \end{aligned} \quad (14)$$

which represent the effects of electron Landau levels in magnetic fields and polarizations of neutron and proton, respectively. Here k_B is the Boltzmann constant, $\mu_{\text{Bn}} = -1.913 \mu_N$, $\mu_{\text{Bp}} = 2.793 \mu_N$ are the magnetic moments of neutrons and protons, respectively, with μ_N being the nuclear magneton, $c_V = 1$, $c_A = 1.26$ are the coupling constants. At the considered densities and temperatures, fermion phase space blocking and dense-medium effects can be safely ignored. The heating rate is given as

$$Q_\nu^+ = \int \sigma_B^{(\text{abs})} c n_n \epsilon_\nu \frac{d^2 n_\nu}{d\epsilon_\nu d\Omega} d\epsilon_\nu d\Omega, \quad (15)$$

where n_n is the number density of neutron, $d^2n_\nu/(d\epsilon_\nu d\Omega)$ is related to the neutrino distribution in the phase space $f(\epsilon_\nu, \Omega)$:

$$\frac{d^2n_\nu}{d\epsilon_\nu d\Omega} = \frac{1}{(hc)^3} f_\nu(\epsilon_\nu, \Omega) \epsilon_\nu^2. \quad (16)$$

Introducing Eq.(16) to (15) yields

$$Q_\nu^+ = \frac{cn_n}{(hc)^3} \int \sigma_B^{(\text{abs})} \epsilon_\nu^3 f_\nu(\epsilon_\nu, \Omega) d\Omega d\epsilon_\nu. \quad (17)$$

Introducing Eq. (11) to (17) yields

$$\begin{aligned} Q_\nu^+ &= \frac{cn_n}{(hc)^3} \int \sigma_0^{(\text{abs})} \epsilon_\nu^3 f_\nu(\epsilon_\nu, \Omega) d\Omega d\epsilon_\nu \\ &\quad + \frac{cn_n}{(hc)^3} \int \sigma_0^{(\text{abs})} \epsilon_{\text{abs}} \hat{\mathbf{n}} \cdot \hat{\mathbf{B}} \epsilon_\nu^3 f_\nu(\epsilon_\nu, \Omega) d\Omega d\epsilon_\nu \\ &\equiv Q_{\nu, B=0}^+ + \Delta Q_{\nu, B \neq 0}^+. \end{aligned} \quad (18)$$

The first term in Eq. (18) can be expressed,

$$Q_{\nu, B=0}^+ = \frac{3c_A^2 + 1}{4} \frac{\sigma_0 c n_n}{(hc)^3} \frac{\langle \epsilon_\nu^2 \rangle}{(m_e c^2)^2} \Omega \int d\epsilon_\nu \epsilon_\nu^3 f_\nu(\epsilon_\nu), \quad (19)$$

where

$$\langle \epsilon_\nu^2 \rangle = \int d\epsilon_\nu \epsilon_\nu^5 f_\nu(\epsilon_\nu) \left(\int d\epsilon_\nu \epsilon_\nu^3 f_\nu(\epsilon_\nu) \right)^{-1}. \quad (20)$$

Here Ω is the solid angle, within which a point outside the neutrino sphere can receive the neutrinos. It is calculated by the geometric calculations (see Figure 4). As stated, the neutrino emission from each point on the neutrino sphere is assumed to be isotropic and take a Fermi distribution with a vanishing chemical potential. The Eq. (19) is expressed with the local neutrino flux, j_ν , which is in turn fixed from the neutrino luminosity obtained in the simulations:

$$Q_{\nu, B=0}^+ = \frac{(3c_A^2 + 1)}{4\pi} \sigma_0 n_n \frac{F_5(0)}{F_3(0)} \frac{(kT_\nu)^2}{(m_e c^2)^2} j_\nu \Omega, \quad (21)$$

where we used the relations,

$$\langle \epsilon_\nu^2 \rangle = F_5(0)/F_3(0)(kT_\nu)^2, \quad (22)$$

with $F_5(0)$ and $F_3(0)$ being the Fermi integrals and

$$\begin{aligned} j_\nu &= c \frac{2\pi}{(hc)^3} \int d\epsilon_\nu \epsilon_\nu^3 f_\nu(\epsilon_\nu) \int_0^1 d\mu \mu \\ &= c \frac{\pi}{(hc)^3} \int d\epsilon_\nu \epsilon_\nu^3 f_\nu(\epsilon_\nu). \end{aligned} \quad (23)$$

By the same procedure as above, the heating rate arising from the parity violating effects can be given as follows,

$$\begin{aligned}
 \Delta Q_{\nu, B \neq 0}^+ &= \frac{3c_A^2 + 1}{4\pi} \sigma_0 n_n \left[\left(\int d\Omega \hat{\mathbf{n}} \cdot \hat{\mathbf{B}} \right) \frac{1}{(m_e c^2)^2} \times \right. \\
 &\quad \left(\frac{1}{2} \hbar c e B \frac{c_V^2 - c_A^2}{c_V^2 + 3c_A^2} - 2 \frac{c_A(c_A + c_V)}{c_V^2 + 3c_A^2} \frac{F_4(0)}{F_3(0)} (\mu_{Bn} B) (k_B T_\nu) \right. \\
 &\quad - 2 \frac{c_A(c_A - c_V)}{c_V^2 + 3c_A^2} \frac{\mu_{Bp} B}{k_B T} \frac{F_5(0)}{F_3(0)} (k_B T_\nu)^2 \\
 &\quad \left. \left. - 2 \frac{c_A(c_A - c_V)}{c_V^2 + 3c_A^2} \frac{F_4(0)}{F_3(0)} (\mu_{Bp} B) (k_B T_\nu) \right) j_\nu \right]. \tag{24}
 \end{aligned}$$

Here $F_4(0)$ is the Fermi integral. The inner product of $\hat{\mathbf{n}} \cdot \hat{\mathbf{B}}$ can be obtained at each point by the geometry.

Using the hydrodynamic quantities at the final time of the numerical simulations (~ 50 msec) as a background, we demonstrate how much the rotation-induced anisotropic neutrino heating can be affected by the parity-violating corrections in the following.

First of all, we take the model SS(U)-2 as an example model. The configuration of the poloidal magnetic fields at the final state is presented in the top left panel of Figure 5. It is seen from the panel that the poloidal magnetic fields are rather straight and parallel to the rotational axis in the regions near the rotational axis, on the other hand, bent in a complex manner, in the other central regions. This can be understood as follows. The core bounce occurs anisotropically due to rotation. This induces the convective motions. The magnetic fields are bent with the convective motions because the magnetic fields are frozen in fluid elements. This is because the ideal MHD is assumed in our simulations. The top right panel of Figure 5 shows the ratio of the neutrino heating rate corrected from the parity-violating effects, $\Delta Q_{\nu, B \neq 0}^+$ to the heating rate without the corrections, $Q_{\nu, B=0}^+$. Note in the panel that the values of the color scale are expressed in percentage and that the central black region represents the region inside the neutrino sphere. It should be remembered that we took the two choices of $T/|W|$ as the initial condition. In the models with the smaller $T/|W| = 10^{-2}$ %, the shapes of the neutrino sphere are found to be rather spherical and the resultant neutrino heating from the neutrino sphere becomes almost isotropic (see the models whose names end with “-2” in the right panel of Figure 3 and Table 3). In such models, it is found that the initial rotation rate and magnetic field are not large enough to make the shapes of the neutrino sphere deviated from being spherically symmetric as in case of the pure rotation (Kotake, Yamada, & Sato 2003). In the top right panel, it is seen that the values of the ratio become negative in almost all the regions (see also the bottom right panel of Figure 5 for clarity). This means that the heating rate is reduced by the magnetic fields than

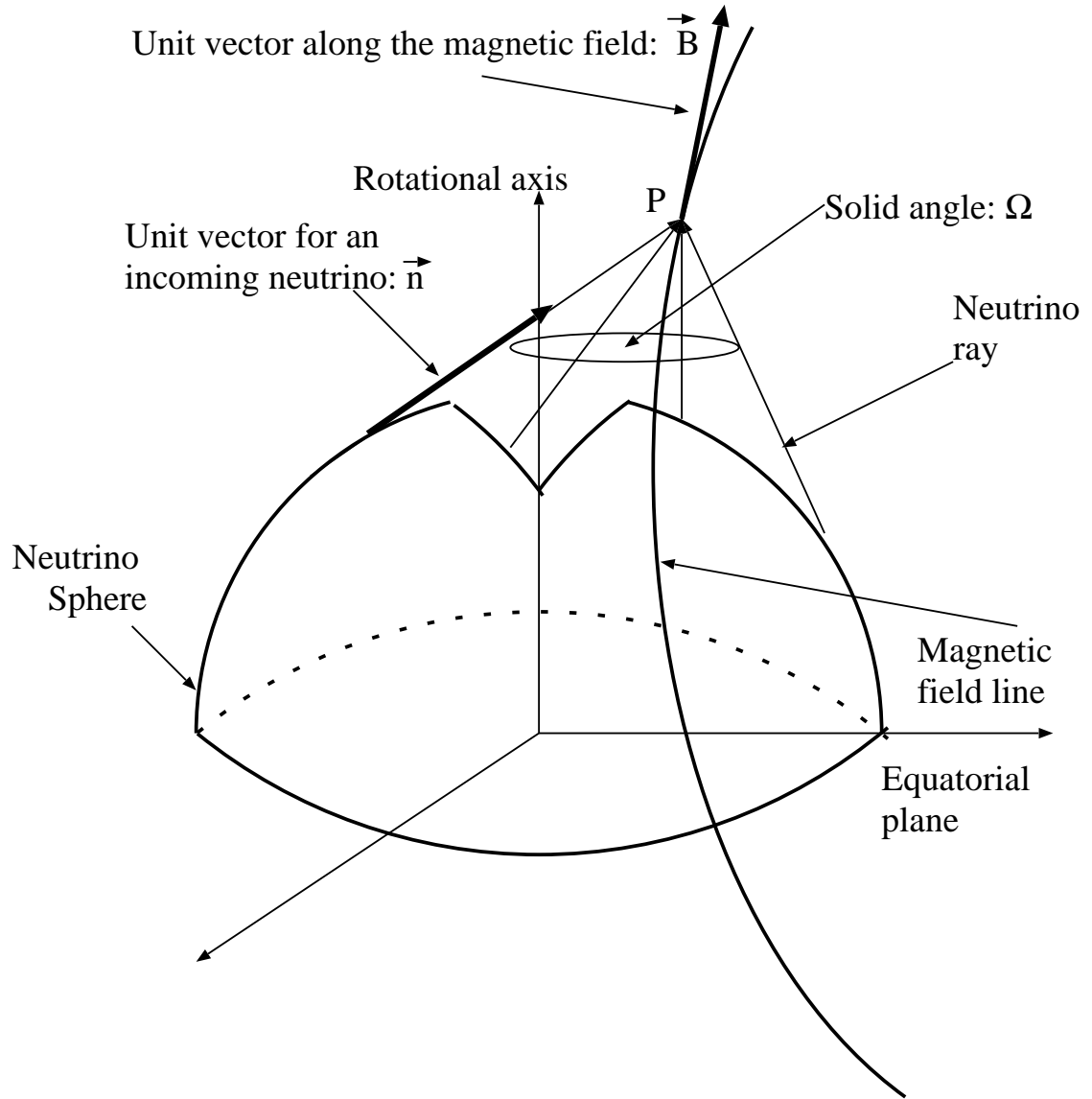


Fig. 4.— Schematic drawing of the analysis scheme of the heating rate. Neutrinos are assumed to be emitted isotropically from each point on the neutrino sphere. The heating rate at P can be found by summing up the contributions of all rays, reaching P .

that without. Especially, this tendency is most remarkable in the regions near the rotational axis and the surface of the neutrino sphere (see the regions colored by blue in the top right panel of Figure 5). These features can be understood as follows. Let us remember that the first term in Eq (24) represents the electron contribution arising from the ground landau level, and the other represents the contribution from the neutron and proton polarizations. By an order-of-magnitude estimation, it can be readily found that the first term dominates over the other in the central core, with typical values of $B \geq 10^{15}$ G, $T \sim O(\text{MeV})$. Since the coefficient of the first term, which is proportional to the coupling constants of weak interactions ($\propto c_V^2 - c_A^2$, where $c_V = 1, c_A = 1.26$) is always negative, then the suppression or the enhancement of the heating rate through parity-violating effects is determined by the signs of the inner product of $\hat{\mathbf{n}} \cdot \hat{\mathbf{B}}$. As mentioned above, the magnetic fields are almost aligned and parallel to the rotational axis in the regions near the rotational axis. With the rather spherical neutrino emission, the values of the inner product becomes positive in the regions, which results in the reduction of the heating rate. On the other hand, the values of the ratio is found to become positive in some regions, where the poloidal magnetic fields are bent due to convections (see the regions colored by red and colored by white in the top and bottom right panels of Figure 5, respectively). In fact, the contributions of the inner product are negative in such regions. In the bottom left panel of Figure 5, the contour of the ratio in the 360 latitudinal degrees region of a star, is prepared in order to see the global asymmetry of the heating. Since our simulations assume the equatorial symmetry, the above features in the northern part of the star become reverse for the southern part. These features on the global asymmetry of the neutrino heating rates are almost common to the other models. In the following, we state some important features of the global asymmetry produced by the difference of the initial rotation rate or the initial configurations of the magnetic fields.

The configurations of the poloidal magnetic fields and the ratio of $\Delta Q_{\nu, B \neq 0}^+ / Q_{\nu, B=0}^+$ for some representative models at the final states are shown in Figure 6. In the models, whose initial profile of the rotation law and the magnetic field is cylindrical with high central concentration (the models whose name has ‘‘CS(NU)’’), the shapes of the shock wave becomes very collimated near the rotational axis (see the bottom left panel of Figure 1). The final profile of the magnetic fields is also centrally concentrated with the strong magnetic fields ($B \sim 4 \times 10^{16}$ G), which is favorable for the heating through parity-violating effects (see the top left and right panels of Figure 6). As a result, the regions, where the equatorial symmetry of the neutrino heating are broken, become rather wider at the north and the south poles than the other models, with the different initial profiles of the rotation and magnetic fields, while fixing the initial strength of rotation. If the initial strength of rotation is more large, the neutrino sphere is deformed to be more oblate due to the centrifugal force (see the black region of the middle right panel of Figure 6). Since the radii of the neutrino spheres tend to

be smaller near the rotational axis than that in the equatorial plane (see Table 3), the solid angle within which a point outside the neutrino sphere receives the rays from the neutrino sphere is enlarged for the vicinity of the rotational axis. This effect makes the neutrino heating near the rotational axis more efficient as in case of pure rotation (Kotake, Yamada, & Sato 2003). This rotation-induced anisotropic neutrino heating enhances the effect of the symmetry of the heating induced by the parity-violating corrections (see the values of R_{mag} in Table 3 and compare the values between the models with the same name except for the final number, for example, SL(U)-2 and SL(U)-1). Furthermore, the regions, which are heated asymmetrically, are enlarged for the faster rotating model than the slower rotating model (compare the top right and the middle right panel of Figure 6).

Finally, we refer to the model whose initial profile of the magnetic field is quadrupole (see the bottom panels of Figure 6). In such models, it is found that there appear the regions with the strong magnetic fields, which seem like the horns, near the rotational axis ranging from $\sim 100 \text{ km} < Z < 200 \text{ km}$ (see the bottom left panel of Figure 6). As a result, the heating regions influenced by the parity-violating corrections, are found to become rather off-axis (see the bottom right panel of Figure 6).

4. Discussion

In our computations, only electron neutrinos are treated approximately. Since all the numerical simulations are limited to rather early phases ($\sim 50 \text{ msec}$), it may not be a bad approximation. However, this is a certain limitation to the study of the later phases, which are more important to investigate the outcome of the north-south neutrino heating asymmetry discussed here. As already mentioned, if we take into the cooling, no heating region is found at these early times. As shown, for example, by Thompson, Burrows, & Pinto (2003), the heating region or (the gain region) appears more than $50 \sim 100 \text{ msec}$ after core bounce. Hence, our estimate of anisotropic neutrino heating is admittedly a bold extrapolation to the later phases, which we have not computed yet. As stated, the multidimensional MHD simulations which solve the neutrino transport with the parity-violating reactions are required in order to compute the relation between the asymmetric neutrino heating induced by the parity-violating corrections and the pulsar-kick. Although we hope that the general features obtained in this study will be taken over later on, further numerical investigations should be required in order to check the validity of our results.

As for the initial configurations of the poloidal magnetic fields, we assume that they have the same profile as the rotation. The assumption may not be unnatural because the angular momentum transfer in quasistatic stellar evolution is tightly connected to the formation of the

magnetic fields (Parker 1979; Spruit 2002). However, multidimensional and self-consistent calculations are required to be done for the understanding of the magnetorotational evolution of supernova progenitors.

5. Conclusion

We performed a series of magnetohydrodynamic simulations of supernova cores. As for the microphysics, we employ a realistic equation of state based on the relativistic mean field theory and take into account electron captures and the neutrino transport via the neutrino leakage scheme. Since the profiles of the angular momentum and the magnetic fields of strongly magnetized stars are still quite uncertain, we constructed 11 initial models changing the combination of the strength of the angular momentum, the rotations law, the degree of differential rotation, and the profiles of the magnetic fields in order to cover as wide a parametric freedom as possible. Based on the numerical simulations, we estimated how the rotation-induced anisotropic neutrino heating is changed by the parity-violating corrections of neutrinos under the strong magnetic fields. By so doing, we investigated the global asymmetry of the neutrino heating in a strongly magnetized supernova core. As a result, we found the following.

1. At the prompt-shock timescale (~ 50 ms after core bounce), the toroidal magnetic fields are formed mainly by the wrapping of the initial poloidal magnetic fields. The strength of the toroidal magnetic fields is smaller than the poloidal ones at the timescale. Although the growth timescale of MRI corresponding to the fastest growing mode of the instability is within the prompt-shock timescale, it is much longer than the growth of the wrapping timescale. The inefficiency of the growth of MRI is due to the initial slow rotation rates prior to core-collapse, which reconciles with the results of the state-of-the-art stellar evolution calculations.

2. Whether the parity-violating corrections in the strong magnetic fields suppress or enhance the heating rate than that without the corrections is found to be simply determined by the inner product of the unit vector of incoming neutrinos ($\hat{\mathbf{n}}$) and the unit vector along the magnetic field direction ($\hat{\mathbf{B}}$). In the models except those with the quadrupole magnetic fields initially, the poloidal magnetic fields near the rotational axis are almost aligned and parallel to the axis at the prompt-shock timescale. Although the neutrino emission is almost spherical in the slowly rotating models with the initial values of $T/|W| = 10^{-2}$ %, the values of the inner product becomes positive in the regions by the geometry of the magnetic field lines. This results in the reduction of the neutrino heating rates. In the faster rotating models with the initial values of $T/|W| = 10^{-1}$ %, the rotation-induced anisotropic neutrino heating

is found to more enhance the asymmetric heating induced by the parity-violating correction than in case of the slower rotating models. This is because the rotation-induced neutrino heating heats the regions near the rotational axis more efficiently, where the magnetic fields are typically strongest. The ratio of the correction to the heating rate to the heating rate without the magnetic fields is found to range from 0.08% to 0.42%.

From the above results, the parity-violating corrections reduces about $\lesssim 0.5\%$ of the heating rate than that without the magnetic fields in the vicinity of the north pole, on the other hand, enhances about $\lesssim 0.5\%$ in the vicinity of the south pole of a star. Based on the results, we speculate that the neutron star might be kicked toward the north pole in the subsequent time, if the asymmetry of the neutrino heating in the north and the south poles develop in the later phases. This is because Scheck et al. (2004). recently pointed out the random velocity perturbation with an amplitude of $\sim 0.1\%$ added artificially at several milliseconds after bounce can be a seed of the global asymmetry of the supernova shock and a cause of the pulsar-kick. In their models. the orientation of pulsar-kicks depends stochastically on the initial random perturbation. This is the case for the observed pulsars with the canonical magnetic fields ($B \sim 10^{12}$ G). However, the asymmetry of the neutrino heating in the strong magnetic fields ($B \geq 10^{15}$ G) considered here might have influence on the alignment of spin and the space velocity of the pulsar associated with the formation of the magnetars. Although no pulsar kicks with the very strong magnetic fields, have been observed so far, the alignment of spin and the space velocity of the magnetars is expected to be observed by future observations.

As stated earlier, our simulations are crude in the treatment of microphysics compared with recent spherical models. This might be justified as long as we study the earlier phase in the prompt-explosion timescale. We are currently developing a two-dimensional neutrino transport code, which will be necessary to test the validity of implications obtained in this study (Kotake et al. 2004 in preparation).

K.K is grateful to K. Sumiyoshi for providing us with the tabulated equation of state, which can be handled without difficulties and to M. Shimizu for supporting computer environments. K.K also thanks H. Sawai and T. Takiwaki for valuable discussions. The numerical calculations were partially done on the supercomputers in RIKEN and KEK (KEK supercomputer Projects No.02-87 and No.03-92). This work was partially supported by Grants-in-Aid for the Scientific Research from the Ministry of Education, Science and Culture of Japan through No.S 14102004, No. 14079202, and No. 14740166.

REFERENCES

- Akiyama, S., Wheeler, J. C., Meier, D. L., & Lichtenstadt, I. 2003, ApJ, 584, 954
- Ardeljan, N. V., Bisnovatyi-Kogan, G. S., & Moiseenko, S. G. 2000, A&A, 355, 1181
- Ardeljan, N. V., Bisnovatyi-Kogan, G. S., & Moiseenko, S. G. 1998, Lecture Notes in Physics, Berlin Springer Verlag, 506, 145
- Arzoumanian, Z., Chernoff, D. F., & Cordes, J. M. 2002, ApJ, 568, 289
- Arras, P. & Lai, D. 1999, ApJ, 519, 745
- Arras, P. & Lai, D. 1999, Phys. Rev. D, 60, 043001
- Balbus, S. A. & Hawley, J. F. 1998, Reviews of Modern Physics, 70, 1
- Bazan, G. & Arnett, D. 1998, ApJ, 496, 316
- Bisnovatyi-Kogan, G. S. & Ruzmaikin, A. A. 1976, Ap&SS, 42, 401
- Bludman, S. A., Lichtenstadt, I., & Hayden, G. 1982, ApJ, 261, 661
- Burrows, A. & Hayes, J. 1996, Physical Review Letters, 76, 352
- Buras, R., Rampp, M., Janka, H.-T., & Kifonidis, K. 2003, Phys. Rev. Lett., 90, 241101
- Cordes, J. M., Wasserman, I., & Blaskiewicz, M. 1990, ApJ, 349, 546
- Duan, H. & Qian Y.-Z. Phys. Rev. D 2004, 69, 123004
- Epstein, R. I. & Pethick, C. J. 1981, ApJ, 243, 1003
- Fryer, C. L. & Warren, M. S. 2004, ApJ, 601, 391
- Fryer, C. L. 2004, ApJ, 601, L175
- Fryer, C. & Kalogera, V. 1997, ApJ, 489, 244
- Goldreich, P., Lai, D., & Sahriling, M. in *Unresolved Problems in Astrophysics*, edited by Bahcall, J. N and Ostriker., J. P. (Princeton University Press, Princeton, 1996)
- Guseinov, O. H., Yazgan, E., Ankey, A., & Tagieva, S. O. 2003, International Journal of Modern Physics D, 1, 1
- Heger, A., Langer, N., & Woosley, S.E. ApJ, 528, 368

- Heger, A., Woosley, S. E., Langer, N., and Spruit, H. C. 2003, to appear in Proc. IAU 215 "Stellar Rotation", (astro-ph/0301374)
- Helfand, D. J., Gotthelf, E. V., & Halpern, J. P. 2001, ApJ, 556, 380
- Horowitz, C. J. & Li, G. 1998, Physical Review Letters, 80, 3694
- Janka, H.-T. & Mueller, E. 1994, A&A, 290, 496
- Janka, H.-T. & Raffelt, G. G. 1999, Phys. Rev. D, 59, 023005
- Kapsi, V. M. et al. 1996, Nature, 381, 584
- Kotake, K., Yamada, S., & Sato, K. 2003, ApJ, 595, 304
- Kotake, K., Sawai, H., Yamada, S., & Sato, K. 2004, ApJ, 608, 391
- Kotake, K., Yamada, S., & Sato, K. 2003, Phys. Rev. D, 68, 044023
- Kotake, K., Yamada, S., Sato, K., Sumiyoshi, K., Ono, H., and Suzuki, H. 2004, Phys. Rev. D, 69, 124004
- Kotake, K., Ohnishi, N., Yamada, S., and Sato, K. in preparation.
- Lai, D., 2004, to appear in 3D Signatures of Stellar Explosion, a workshop honoring J.C. Wheeler's 60th Birthday
- Lai, D., Chernoff, D. F., & Cordes, J. M. 2001, ApJ, 549, 1111
- LeBlanc, J.M., & Wilson, J.R. 1970, ApJ, 161 ,541
- Liebendörfer, M., Mezzacappa, A., Thilemann, F.-K., Messer, O.E.B., Hix, W.R., and Bruenn, S.W. 2001, Phys. Rev. D, 63, 103004
- Liebendörfer, M., Rampp, M., Janka,H.-T., and Mezzacappa, A. 2003, submitted to ApJ
- Liebendörfer, M., Pen, U.-L., and Thompson, C. 2004, submitted to Nucl. Phys. A, astro-ph/0408161
- Lorimer, D. R., Bailes, M., & Harrison, P. A. 1997, MNRAS, 289, 592
- Lyne, A. G., Lorimer, D. R. 1994, 369, 127
- Mirabel, I. F., Mignani, R., Rodrigues, I., Combi, J. A., Rodríguez, L. F., & Guglielmetti, F. 2002, A&A, 395, 595

- Müller, E. & Hillebrandt, W. 1979, *A&A*, 80, 147
- Müller, E., Rampp, M., Buras, R., Janka, H.-T., & Shoemaker, D. H. 2004, *ApJ*, 603, 221
- Ott, C. D., Burrows, A., Livne, E., & Walder, R. 2003, submitted to *ApJ*, (astro-ph/0307472)
- Parker, E. N. 1979, *Cosmological magnetic fields: The origin and their activity* (Oxford, Clarendon Press)
- Pavlov, G. G., Kargaltsev, O. Y., Sanwal, D., & Garmire, G. P. 2001, *ApJ*, 554, L189
- Rampp, M. & Janka, H.-T. 2000, *ApJ*, 539, L33
- Symbalisty, E. 1984, *ApJ*, 285, 729
- Shen, H., Toki, H., Oyamatsu, K., Sumiyoshi, K. 1998, *Nuclear Physics*, A637, 43, 109, 301
- Scheck, L., Plewa, T., Janka, H.-T., Kifonidis, K., & Müller, E. 2004, *Physical Review Letters*, 92, 011103
- Stone, J. M. & Norman, M. L. 1992, *ApJS*, 80, 753
- Spruit, H. C. 2002, *A & A*, 381, 923
- Takiwaki, T., Kotake, K., S. Nagataki., and Sato, K. 2004, *ApJ* in press
- Thompson, T. A., Burrows, A., & Pinto, P. A. 2003, *ApJ*, 592, 434
- van Riper, K. A. & Lattimer, J. M. 1981, *ApJ*, 249, 270
- van Riper, K. A. 1982, *ApJ*, 257, 793
- Wex, N., Kalogera, V., & Kramer, M. 2000, *ApJ*, 528, 401
- Yamada, S. & Sawai, H. 2004, *ApJ*, 608, 907
- Yamada, S., Kotake, K., & Yamasaki, T. 2004, *New. J. Phys*, 6, 79
- Zhang, B. & Harding, A. K. 2000, *ApJ*, 535, L51

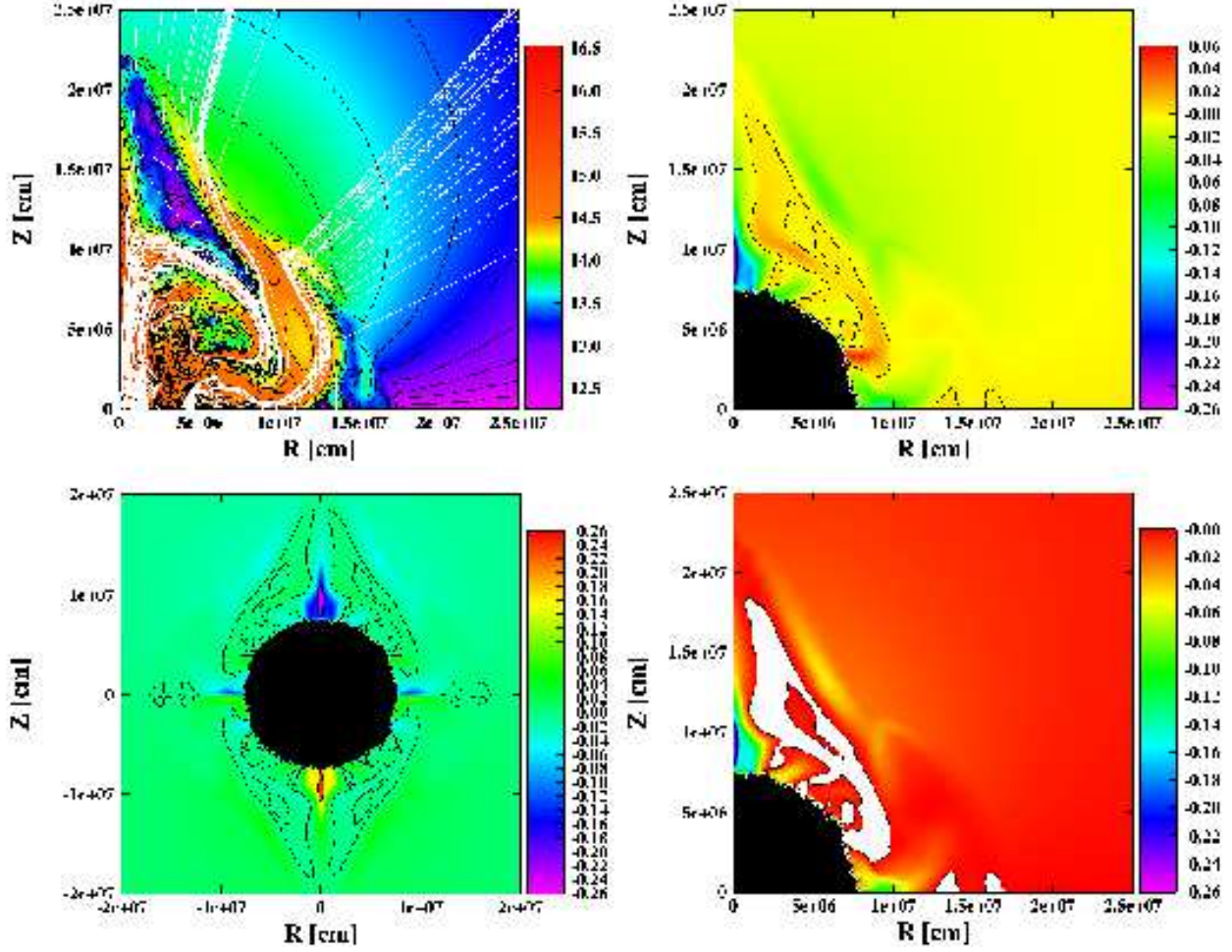


Fig. 5.— Various quantities for the model SSU-2. Top left panel shows contour of the logarithm of the poloidal magnetic fields ($\log[B_p \text{ (G)}]$) with the magnetic field lines. Top right panel represents the ratio of the neutrino heating rate corrected from the parity-violating effects, $\Delta Q_{\nu, B \neq 0}^+$ to the heating rate without the corrections, $Q_{\nu, B=0}^+$. Note in the panel that the values of the color scale are expressed in percentage and that the central black region represents the region inside the neutrino sphere. Bottom right panel is the same with the top right panel except that the bottom right panel only shows the regions with the negative values of the ratio. Thus the white region shows the regions with the positive values of the ratio. Bottom left panel shows the contour of the ratio in the whole region, which is prepared in order to see the global asymmetry of the heating induced by the strong magnetic fields.

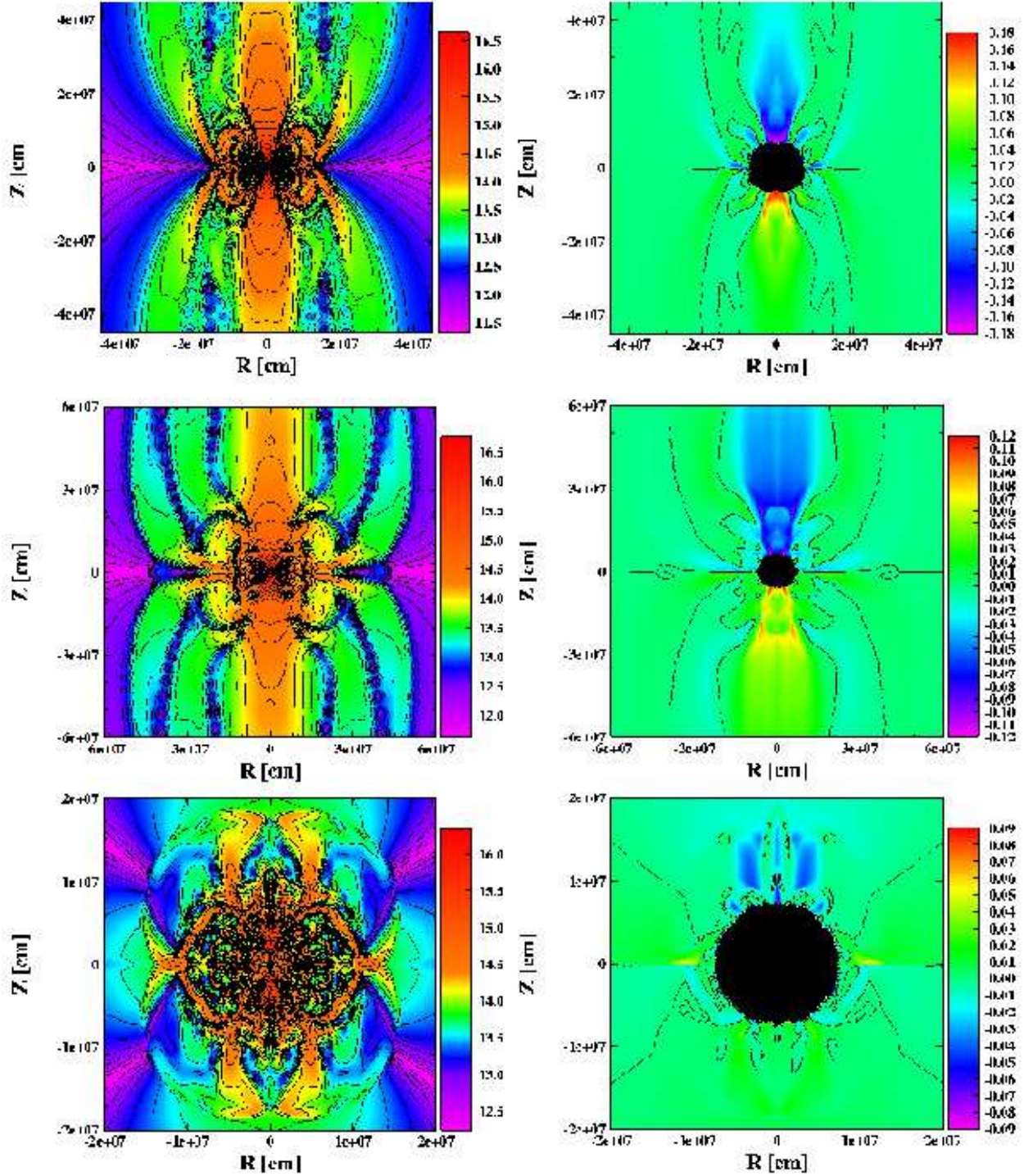


Fig. 6.— The contour of the logarithm of the poloidal magnetic fields (G) (left panels) and the contour of $\Delta Q_{\nu, B \neq 0}^+ / Q_{\nu, B = 0}^+$ in percentage (right panels). The top, middle, and bottom panels, correspond to the models CS(NU)-2, SS(NU)-1, and CS(Q)-2, respectively.